Active site loop dynamics of a class IIa fructose 1,6-bisphosphate aldolase from *M. tuberculosis*

Scott D. Pegan[1,*], **Kamolchanok Rukseree**[2,3], **Glenn C. Capodagli**[1], **Erica A Baker**[1], **Olga Krasnykh**[3,4], **Scott G Franzblau**[3,4], and **Andrew D Mesecar**[5,*]

[1]Eleanor Roosevelt Institute and Department of Chemistry and Biochemistry, the University of Denver, 80208

[2]National Center for Genetic Engineering and Biotechnology (BIOTEC), NSTDA, Thailand Science Park, 12120

[3]Institute for Tuberculosis Research, the University of Illinois at Chicago, 60612

[4]Department of Medicinal Chemistry, the University of Illinois at Chicago, 60607

[5]Department of Biological Sciences and Chemistry and the Purdue Center for Cancer Research, Purdue University, West Lafayette, IN 47907, USA

Abstract

Class II fructose 1,6-bisphosphate aldolases (FBA; E.C. 4.1.2.13) comprise one of two families of aldolases. Instead of forming a Schiff-base intermediate using an ε-amino group of a lysine side chain, class II FBAs utilize Zn(II) to stabilize a proposed hydroxyenolate intermediate (HEI) in the reversible cleavage of fructose 1,6-bisphosphate forming glyceraldehyde 3-phosphate and dihydroxyacetone phosphate (DHAP). As class II FBAs has been shown to be essential in pathogenic bacteria, focus has been placed on these enzymes as potential antibacterial targets. Although structural studies on class II FBAs from *Mycobacterium tuberculosis* (MtFBA), other bacteria and protozoa have been reported, the structure of the active site loop responsible for catalyzing the protonation/deprotonation steps of the reaction for class II FBAs has not yet been observed. We therefore utilized the potent class II FBA inhibitor phosphoglycolohydroxamate (PGH) as a mimic of the HEI/DHAP bound form of the enzyme and determined the X-ray structure of MtFBA-PGH complex to 1.58 Å. Remarkably, we are able to observe well-defined electron density for the previously elusive active site loop of MtFBA trapped in a catalytically competent orientation. Utilization of this structural information plus site-directed mutagenesis and kinetic studies conducted on a series of residues within the active-site loop revealed that E169

[*]Correspondence addressed to Department of Biological Sciences and the Purdue Center for Cancer Research, Purdue University, West Lafayette, IN 47907 (ADM) or Eleanor Roosevelt Institute and Department of Chemistry and Biochemistry, University of Denver, 2190 E. Iliff Ave, Olin 202, Denver, CO 80208 (SDP). Tel: (312) 996-1877 (ADM) or (303) 871 2533 (SDP); amesecar@purdue.edu (ADM) or spegan@du.edu (SDP).

SUPPORTING INFORMATION AVAILABLE

A view of the MtFBA active site loop with its associated electron density shown as an F_O-F_C omit map, $2F_O$-F_C simulated annealed map and F_O-F_C simulated annealing map can be found in supplementary figure 1. Also, the location of MtFBA-PGH active site loop in relation to the MtFBA-PGH tetramer can be found in supplementary figure 2. This material is available free of charge via the Internet at http://pubs.acs.org.

The atomic coordinates and structure factors have been deposited with the Brookhaven Protein Data Bank (PDB codes 4DEF, 4DEL).

facilitates a water mediated deprotonation/protonation step of the MtFBA reaction mechanism. Also, secondary isotope effects on MtFBA and catalytically relevant mutants were used to probe the effect of loop flexibility on catalytic efficiency. Additionally, we also reveal the structure of MtFBA in its holoenzyme form.

Class II fructose 1,6-bisphosphate aldolase (FBA; E.C. 4.1.2.13) catalyzes the second reversible step of the glycolytic pathway in the majority of protozoa, bacteria, fungi, and blue-green algae[1]. In doing so, FBA generates glyceraldehyde 3-phosphate (G3P) and dihydroxyacetone phosphate (DHAP) from the cleavage of the open-chain form of fructose 1,6 bisphosphate (FBP; Figure 1). With DHAP rapidly converted to an additional G3P molecule by triosephosphate isomerase (E.C. 5.3.1.1), FBAs are critical for supplying downstream metabolic enzymes with G3P. In the reversible reaction when gluconeogensis is required, class II FBAs perform an adol condensation of DHAP and G3P to produce FBP (Figure 1)[2]. Together, the substrates and products that this class II FBAs supply, are crucial for any an organism's survival.

Class II FBAs are one of two families of aldolases. Both class II FBA and class I FBAs are proposed to have evolved independently from a common ancestor as they are all comprised of similar α/β folds[3, 4]. Despite their common structural folds and tendencies to form dimeric or higher order quaternary structures, class I and class II FBAs are strikingly different. Whereas class I FBAs utilize the ε-amino group of a lysine side chain to form a Schiff-base intermediate during the reaction mechanism, class II FBAs require metal cations for catalysis including an active site Zn(II) that stabilizes a putative hydroxyenolate intermediate (HEI). Additionally, class II FBAs are activated by monovalent cations, whereas class I FBAs have no such activation[1, 3, 5].

In addition to differing in reaction mechanism, class I and II FBAs also differ in their distribution across species. Mammals rely on class I FBA for metabolism, while class II FBAs are present only in protozoa, bacteria, fungi and blue-green algae. This distribution has prompted several investigations on whether class II FBAs are essential for microbial survival, particularly in bacterium that possess both class I and class II FBAs. Supporting this assertion, FBA gene, *fbaB* (class I) knockout strains derived from bacterium autotrophic for both genes have been successfully obtained[6, 7]. However, attempts to knockout the *fbaA* gene (class II) in *Mycobacterium tuberculosis, Escherichia coli, and Streptomyces galbus*, all of which contain both classes of FBA, resulted in non-viable bacteria [2, 6, 8, 9]. Also, only significant bacterial expression levels of class I FBAs have been observed in the presence of gluconeogenic substrates or high aeration conditions[10, 11]. These results, along with up-regulation of the class II FBA gene in *M. tuberculosis* under hypoxic conditions, suggest that class II FBAs are essential for bacterial survival[12].

One of the prokaryotic class II FBAs that has been of recent focus is that from *M. tuberculosis*, the causative agent for tuberculosis[2, 13]. Tuberculosis is one of the leading causes of mortality in developing countries and one-third of the world's population is predicted to harbor the bacterium[14]. With the emergence of the so-called "extensively" drug-resistant strains of *M. tuberculosis*, a new urgency exists for the development of novel therapeutics, and the class II FBA from *M. tuberculosis* (MtFBA) may serve as a new

target[15]. MtFBA belongs to one of two class II subfamilies designated as class IIa. Members within each subfamily share 40% sequence homology compared to 25%-30% across all class II FBAs.

We previously determined the high resolution X-ray structures of MtFBA bound with DHAP, DHAP-G3P and FBP, and these structures provided unique insight into the interactions of MtFBA with its substrates and into the reaction mechanism of this enzyme at the atomic level[2]. In addition, these structures also allowed us to visualize the putative hydroxyenolate intermediate (HEI) of the reaction, which was also the theoretical basis for the design of the first potent inhibitor of class II FBAs, phosphoglycolohydroxamate (PGH) [16]. PGH has been shown to be a potent inhibitor of class II FBAs with measured K_i values of 37 nM, 11 nM, and 20-50 nM for class II FBAs from *Giardia lambia, Saccharomyces cerevisiae, Escherichia coli* respectively [16-18]. Although we have reported the X-ray structures of MtFBA with its substrates and products, and the X-ray structures of the class IIa FBA enzyme from *E. coli* (EcFBA) and the class IIb FBAs from *G. lambia* (GlFBA), *Thermus aquaticus* (TaFBA), and *Helicobacter pylori* (HpFBA) are also known, the structural and thermodynamic basis for the potency of PGH has yet to be fully determined[2, 13, 19-21]. This is in large part because all of the previously reported structures of class II FBAs are missing electron density for a catalytically important loop that contains an essential glutamate residue that is proposed to be directly involved in the protonation/deprotonation step of the MtFBA-mediated reaction (Figure 1)[22].

Since PGH is proposed to mimic the DHAP/HEI intermediate step of the FBA reaction where an amino acid residue would be required to act, either directly or indirectly through a water molecule, to deprotonate/protonate (step II, Figure 1), we determined the X-ray structure of PGH bound to MtFBA in an attempt to trap the active site loop in a catalytically relevant conformation. We also determined the X-ray structure of the zinc-bound, substrate-free form of MtFBA that proves that this catalytically required divalent metal cation is capable of binding to the free enzyme in contrast to another report[9]. Based on these structures, and those of MtFBA in complex with DHAP, DHAP-G3P and FBP that we previously determined, we performed site-directed mutagenesis and kinetic studies to identify and more fully elucidate the roles this catalytically relevant glutamate residue with respect to its interaction with PGH. Interestingly, this interaction occurs through a coordinated water molecule via a shuttle mechanism, likely mimicking its orientation during the protonation/deprotonation step of the MtFBA reaction mechanism. Finally, we probed the importance of several residues within the active site loop on the catalytic efficiency of MtFBA.

EXPERIMENTAL PROCEDURES

Materials

Chemicals, biochemicals, buffers, and solvents were purchased from Sigma-Aldrich Chemical Co. (St. Louis, MO), Fisher Scientific Inc. (Pittsburgh, PA), Fluka Chemical Corp. (Milwaukee, WI), or EM Science (Cincinnati, OH). Specifically for enzymatic assays, β-Nicotinamide adenine dinucleotide, reduced dipotassium salt (NADH; Sigma N4505), Nicotinamide adenine dinucleotide hydrate (NAD+; Sigma 43407), α-glycerophosphate

dehydrogenase (Sigma G6880), rabbit muscle triosephosphate isomerase (TIM, Sigma T6258), rabbit glyceraldehyde 3-phosphate dehydrogenase (GAPDH; Sigma G2267), D-fructose 1,6-bisphosphate tetra(cyclohexylammonium) salt (FBP; Sigma F0752), and dihydroxyacetone phosphate dilithium salt (DHAP; Sigma D7137) were used. The Vivaspin centrifugal filter devices were obtained from GE Healthcare (Piscataway, NJ). The Ni-NTA and the Superdex-S200 High Resolution resins were obtained from Qiagen (Valencia, CA) and GE Healthcare (Piscataway, NJ) respectively. Enzymes and reagents used for molecular biology procedures were obtained from Fermentas, Inc. (Glen Burnie, MD), Qiagen (Valencia, CA), and Agilent Technologies (Santa Clara, CA).

Synthesis of phosphoglycolohydroxamate

Phosphoglycolamide (PGA), a precursor of PGH, and PGH itself, was prepared from glycolamide according to a published procedure which uses available and inexpensive reagents, with minor modifications[23]. The first step (phosporylation of glycolamide by polyphosphoric acid) was carried out at 44-48°C. The reaction mixture was cooled; water and ice were added to the reaction mixture under vigorous stirring conditions to prevent pH fluctuations, which can lead to decomposition. Solid $Ba(OH)_2$ and $BaCO_3$ were then added in small portions until pH~8 was achieved. The resulting precipitate was filtered off with the filtrate subsequently being concentrated under reduced pressure. After cooling at 4°C, resulting crystals of barium salt of PGA (first portion) were filtered out, washed with a cold mixture of ethanol and water, then dried in the vacuum dessicator over P_2O_5. The inorganic barium salt precipitates were washed with a small amount of cold water and filtered. The resulting aqueous solution was concentrated; providing a second portion of barium salt of PGA, which was treated similarly to the first. A Dowex 50×4 (H^+) (exchange capacity 1.2 meq/ml) was used to obtain PGA from its barium salt (approximately 2 equivalents of resin for 1 equivalent of salt).

For PGH synthesis, the water solution of PGA (after resin was filtered off) was treated with 15 equivalents of hydroxylamine (50 % w/v solution in water), with the reaction mixture kept overnight at room temperature, evaporated under vacuum, dried additionally in high vacuum and used for preparing PGH-CHA salt without additional purification. The PGH was dissolved in water (approximately 30 mg/mL) and 6 equivalents of cyclohexylamine were added under stirring, evaporated in vacuum, then recrystallized from ethanol. Cyclohexylamine was preferred to the barium salt to avoid barium contamination of the MtFBA active site. To ensure the quality of the resulting PGH-CHA salt, H^1-NMR spectra were recorded at 400 MHz on Bruker DPX-400 spectrometer for 28 mg/mL solution in D_2O. ^1H NMR δ: 0.95-1.30 m (10H), 1.44-1.94 m (10H), 3.02 m (2H) (all – cyclohexyl); 4.18 d (*J*= 7 Hz, 2H, CH_2); 4.69 (H_2O). ^{13}C NMR δ: 23.35, 23.84, 29.89, 49.87 (cyclohexyl); 62.02, 62.87 (CH_2), 169.30, 162.22 (C=O). ^{31}P NMR δ: 3.55.

MtFBA expression vector and site-directed mutagenesis of the fba gene

The construction of the *M. tuberculosis* pET17b-*fba*H expression vector harboring the *fba* gene (Rv0363c) was previously described [2]. The expression system produces a C-terminal, His-tagged fusion protein, which is referred to herein as MtFBA. The residual His-tag has been observed not to affect the overall structure of MtFBA or its *in vitro* activity[2, 9, 24].

Mutations in MtFBA were incorporated via the Quick-Change Site-directed Mutagenesis system (Agilent Technologies). The following oligonucleotides were used for mutatagenesis with the altered bases in bold: 5'-CGGCGTCGTCGCCGCCGAAGAGGACG-3' (G166A/G167A), 5'-CGGCGTCGTCGGCGCCGAAGAGGACG-3' (G167A), 5'-CGTCGGCGGCGCAGAGGACGGCG-3' (E168A), and 5'-CGGCGGCGAAGCGGACGGCGTGG-3' (E169A). The resulting pET-fbaH mutant plasmids were introduced into *E. coli* XL-1 blue cells by heat-shock transformation and were then propagated and purified in large scale for sequence verification and transformation into *E. coli* BL21 (DE3) for enzyme expression. The complete coding regions for all mutant enzymes were sequenced using either the RRC DNA sequencing facility at the University of Illinois, Chicago or CU Cancer Center DNA Sequencing & Analysis Service.

Production and purification of wild type and mutant MtFBA

E. coli BL21 (DE3) harboring either wild-type or mutant pET-*fba*H were grown at 37 °C in 8 liters (8 × 1 liter) of LB broth containing 100 μg/mL of ampicillin until the OD_{600} was approximately 0.6. Expression of the *fba*H gene was induced by the addition of IPTG to a final concentration of 0.4 mM and the culture was allowed to grow for another 4-6 h at 25 °C. After this time period, bacterial cells were harvested by centrifugation at 3000×g for 15 min. Cells were washed with PBS and stored at -20 °C until use. The cell pellets collected from the 8-L culture were suspended in buffer A (50 mM sodium phosphate buffer, pH 8.0, and 300 mM NaCl) and subsequently lysed by the addition of 5 mg of chicken lysozyme followed by sonication using a Gex 600 Ultrasonic Processor (Footswitch). Sonication pulse settings were 5 s on and 5 s off for a total on time of 5 minutes at 60% amplitude. Insoluble cell debris was removed by centrifugation at 16,000 ×g for 45 min at 4 °C. MtFBA was purified from the soluble fraction by nickel affinity and size exclusion according to our previously described methods[2]. The resulting purified wild type and mutant MtFBA enzymes were exchanged into buffer B (20 mM Tricine buffer pH 8, 100 mM NaCl, 0.1 mM $ZnCl_2$ and 2 mM DTT) and then concentrated to 15 mg/mL using ultrafiltration units fitted with 10 kD MWCO filters (GE Healthcare). The final protein was also filtered through 0.65 μm membrane filters to remove any precipitate. After purification, the concentrations of all proteins were determined by absorbance at 280 nm using molar extinction coefficients experimentally derived by the method of Gill & von Hippel, 23,044 M^{-1} cm^{-1} or 0.619 L g^{-1} cm^{-1} [25].

Isothermal Titration Calorimetry (ITC) Experiments

ITC experiments were conducted using a VP-ITC system (Microcal, Amherst, MA). Degassed protein samples for wild type and G166A/G167A MtFBA were used and titrations were performed at 25.2°C. Prior to degassing, both proteins were dialyzed against a solution of 50mM Tricine 7.5, 100 mM NaCl, 0.1 mM $ZnCl_2$, 2 mM DTT. Isothermal titrations of wild type MtFBA with PGH were performed in duplicate and were comprised of 60 (1.5 μl) injections of 2 mM PGH into 80 μM of wild type MtFBA. Isothermal titrations of wild type MtFBA with DHAP were performed using the same experimental parameters as those with PGH except that PGH was substituted for 2 mM DHAP. Time delays between injections were set at 300 s for the initial delay and then 200 s in between subsequent injections.

Isothermal titrations of G166A/G167A MtFBA with PGH were performed with 60 μM of protein and with delay times between injections of 500 s. All other parameters remained the same as with wild type MFBA. The average heat released (kcal/mole of injectant) of the last 5 injections was used to correct for the heat of dilution. All ITC data sets were analyzed and fit to a single-site binding model using non-linear curve fitting procedures in the MicroCal Systems software (ORIGIN 5.0).

MtFBA Enzymatic FBP Cleavage Assays

The coupled assay for the FBP cleavage activity of FBA was carried out as described previously with slight modifications[4]. The assay mixture (final volume 100 μL) contained 0.4 mM NADH, 2 U/mL of rabbit muscle α-glycerophosphate dehydrogenase, 20 U/mL of rabbit muscle TIM, 0.02% (w/v) BSA, 100 mM potassium acetate and 100 mM Tris-HCl, pH 7.8, and the wild type and mutant MtFBAs (0.134, 0.537 (E168A), 161 (E169A), 10.7 (G167A), 10.7 (G166A/G167A), and 0.269 (D276A) μM). The reaction was initiated by the addition of FBP (final concentration ranging from 0-2000 μM). All assays were performed at room temperature and in triplicate using 96-well, flat-bottom polystyrene plates (Fisherbrand). All MtFBA activity assays were recorded using a Molecular Devices SpectraMax384 Plus plate reader by measuring the decrease in NADH absorbance at 340 nm ($\varepsilon = 6,220$ M^{-1} cm^{-1}). The path length for the assay was determined to be 0.36 cm. To determine the kinetic parameters V_{max} and K_m, rates were derived from initial velocity data were fit to the Michaelis-Menten equation, $\upsilon = V_{max}/(1+(K_m/[S]))$, using the Enzyme Kinetics Module 1.3 of Sigma Plot version 10 (SPSS Inc.). Values for k_{cat} were calculated from V_{max} using the total enzyme concentration [E] via the equation $k_{cat} = V_{max}/[E]$. One unit of aldolase activity is defined as the amount of enzyme that catalyzes the cleavage of 1 μmol of FBP per min under the conditions of the assay. All turnover number (k_{cat}) values were calculated using the concentration of a monomer of MtFBA.

Solvent Isotope Effects

To evaluate the solvent (D_2O) kinetic solvent isotope effects on the MtFBA reaction, enzyme activity measurements were performed in a reaction mixture containing greater than 94.5% D_2O concentration. This was achieved by bringing up all of the assay reagents in 99.9% D_2O (Sigma 364312). To minimize the amount of H^+ in solution, all reagent solutions were generated from anhydrous salts, or lyophilized enzymes, just prior to the assay to ensure minimal water exchange with air. Additionally, wild type and mutant MtFBAs were diluted to their working stock concentrations in D_2O. This minimized the only source of H_2O to negligible carry over from the purification of MtFBAs themselves and the 10 μL of the buffer that was used, which in comprises only 5.5% of the assays volume. The relation of pH to pD was determined using pH = pD + 0.4 [26]. The activity of MtFBA at the resulting pD value, 7.4, is predicted to fall within approximately 15% of that at its optimal pH, 7.8[4].

IC$_{50}$ determination of PGH

The affinity of PGH to MtFBA was estimated by determining the IC$_{50}$ value for the interaction. The experimental conditions used were the same as those for determining the

K_m values for FBP with the exception that PGH concentrations were varied from (0-20 μM) at a fixed FBP concentration of 40 μM (the K_m value for FBP). To determined the IC_{50} value for PGH, the percent inhibition (I%) was calculated using the following formula, I% = $(1-(\upsilon_{sample}-\upsilon_{negative\ control})/ (\upsilon_{positive\ control}-\upsilon_{negative\ control})) \times 100$. The resulting I% values were plotted as a function of PGH concentration and the data were fit via non-linear regression to the equation, I% = $(I\%_{max}/(1+(IC_{50}/[PGH])))$.

K_i determination of DHAP

For determination of the K_i value for DHAP, we had to modify the MtFBA enzymatic cleavage assay to prevent degradation of DHAP[21]. To achieve this, rabbit muscle α-glycerophosphate dehydrogenase was replaced with rabbit GAPDH to couple MtFBA produced G3P to the reduction of NAD+. Thus, MtFBA activity was observed through an increase in absorbance at 340 nm. Furthermore, TIM was removed and potassium arsenate added to mimic phosphate as a GAPDH co-substrate. The final assay mixture contained 0.2 mM NAD+, 5 U/mL of rabbit GAPDH, 0.02% (w/v) BSA, 100 mM potassium acetate, 5 mM potassium arsenate and 100 mM Tris-HCl, pH 7.8, and the 0.002 mg/mL wild type MtFBA. MtFBA inhibition studies with DHAP as the varied substrate were carried out using five DHAP concentrations, spanning from 0-4,000 μM, and four FBP concentrations spanning 8-80 μM. Initial velocity data were fit, using non-linear regression analysis, to each of the equations describing partial and full models of competitive, uncompetitive, noncompetitive, and mixed inhibition using the in Enzyme Kinetics Module (version 1.3) of Sigma Plot (Version 10, SPSS Inc.). Based on analysis of fits through "Goodness-of-fit" statistics, the full competitive inhibition model with the following equation, $\upsilon = V_{max}/(1+ (K_m/[S])(1+([I]/K_i)))$, was found to best-fit the kinetic inhibition data. Here, [S] = [DHAP], [I] = [FBP] and Ki is the dissociation constant of FPB from free MtFBA.

MtFBA and MtFBA-PGH Crystallization

Initial co-crystallization conditions for the MtFBA-PGH complex were achieved using conditions from our previously described crystallization protocols[2]. Final co-crystals of the MtFBA-PGH complex structure were grown using hanging-drop vapor diffusion at room temperature. Crystallization drops included 4 μL of a 15 mg/mL MtFBA protein solution containing Buffer B and 2 mM PGH (cyclohexylammonium salt) that was mixed in a 1:1 ratio with a precipitant of 26% PEG 300 and 0.1 M sodium acetate, pH 4.8. Crystals appeared within 4-5 days. MtFBA crystals without PGH were grown using the same protocol used for MtFBA-PGH crystal growth except that a 26%-32% PEG 300 gradient was used instead. We found that the addition of 2% (w/v) DMSO as an additive caused MtFBA-holo crystals to form sporadically after 4-6 wks.

X-ray Structural Determination of MtFBA and MtFBA-PGH Complex

X-ray data sets for MtFBA-PGH were collected at SER-CAT beam line 22-ID, while X-ray data sets for MtFBA-apo were collected at LS-CAT beam line 21-ID-D. All crystals were mounted on nylon loops and submerged in a 5 μL volume of mother liquor as a cryo solution. Crystals were subsequently flash-cooled in liquid nitrogen and mounted under a stream of dry N_2 at 100 °K. All data sets were collected from a series of 0.5 degree rotational X-ray frames using a MAR 300 CCD detector. X-ray images were indexed,

processed, integrated and scaled together using the program HKL2000[27]. Since the MtFBA and MtFBA-PGH proteins crystallized in the same space group (I222) with similar unit cell dimensions as those of the MtFBA-substrate complexes, initial phases were readily obtained via rigid-body refinement using the program Refmac 6.2 and the MtFBA-DHAP (3ekl) structure without DHAP as a starting model[2, 28]. The program WinCoot was used for model building, and Refmac 6.2 from the CCP4 suite was used for refinement[28]. Coordinates and molecular library files for the ligand PGH were generated using the program Sketcher in the CCP4 program suite. Isotropic temperature factors were refined and occupancies were 1.00 for all atoms of the MtFBA-PGH and MtFBA-apo structures. Water molecules were added to F_o-F_c density peaks that were greater than 3σ using the "Find Water" winCoot program function. The final models were checked for structural quality using the CCP4 suite programs Procheck and Sfcheck. The atomic coordinates and structure factors have been deposited with the Brookhaven Protein Data Bank (PDB codes 4DEF, 4DEL). Simulated annealing F_o-F_c and $2F_o$-F_c density maps were generated by Phenix version 1.8.1-1168[29].

RESULTS

Binding affinity of PGH and DHAP for MtFBA

Since PGH has been shown to be a potent inhibitor of FBA from other species, we wanted to directly determine the dissociation constants (K_d and K_i values) for PGH and DHAP with MtFBA. Isothermal titrations of MtFBA with PGH and DHAP were performed and revealed that only the binding of PGH involves an enthalpic (H) component as no heat was detected for the interaction between MtFBA and DHAP (Figure 2ab). The resulting thermodynamic constants for the interaction of PGH per MtFBA monomer are; H= -9,354 ± 8 cal/mol, S= 3.75 ± 0.02 cal mole^{-1} K^{-1}, and K_d= 21.1 ± 0.2 nM with n=0.90 ± 0.04, for PGH (Figure 2b). The absence of an enthalpic contribution to DHAP binding suggested that an additional interaction might be stabilized by PGH beyond those interactions found between DHAP and MtFBA. The similarities between the chemical structure of DHAP and PGH, along with the recently revealed MtFBA-DHAP/HEI structure, suggested that the stabilization of the active site loop might be the source of the heat observed (Figure 2b). To explore the potential link between the active site loop and the heat observed, ITC was performed on a loop stabilizing double MtFBA mutant, G166A/G167A (Figure 2c). Although still possessing all its catalytic residues, no heat was detected for G166A/G167A's interaction with PGH supporting the divergent relationship between PGH and DHAP in regards to the residues these molecules interact with in the active site loop.

Since we could not determine directly the K_d value for the binding of DHAP to MtFBA, we focused on determining the relative affinity of DHAP for MtFBA by measuring its inhibition constant (K_i) against FBP in the forward reaction. We utilized a modified version of the absorbance-based enzymatic assay that was previously used for GlFBA kinetic characterization[21]. This assay utilizes glyceraldehyde 3-phosphate dehydrogenase (GAPDH) to couple MtFBA generated G3P to the reduction of NAD+ to NADH. Additionally, the coupling enzyme TIM was removed from the assay to prevent the conversion of DHAP to G3P. Four different fructose 1,6-biphosphate concentrations and

five different DHAP concentrations were utilized to determine the kinetic response of MtFBA to varying concentrations of substrate and the product inhibitor DHAP. The results of the kinetic studies are shown in Figure 2d as a Lineweaver-Burk plot. The pattern in the data indicates that DHAP behaves as a competitive product inhibitor against the substrate fructose 1,6-biphosphate with a K_i value of 238 ± 20 μM for MtFBA. This mode of inhibition is consistent with the product G3P leaving first followed by DHAP in a uni-bi kinetic scheme. This mechanism of product release also supports our previous X-ray structural data for the MtFBA-DHAP complex where we observe DHAP binding deep within the enzyme's active site pocket preventing FBP from accessing the active site zinc and catalytic relevant residues[2]. These results indicate that PGH binds to MtFBA approximately 11,000 times more tightly than DHAP.

X-ray structure of the MtFBA-PGH complex

The observation that PGH binds to MtFBA approximately 10^4-times stronger than DHAP with a strong enthalpic contribution to binding, and the observed absence of heat involved the interaction with DHAP, suggests that significantly different structural interactions must exist between the MtFBA-DHAP and MtFBA-PGH complexes. Therefore, we co-crystallized MtFBA with the inhibitor PGH, Zn^{2+} and Na^+ under conditions similar to those used to obtain crystals of the MtFBA-DHAP complex and determined its structure to 1.58 Å resolution (Table 1)[2].

Analysis of the conformation of the biologically relevant tetramer within unit cell revealed that the overall conformation of the enzyme and crystal packing geometry are essentially the same as those observed previously for the X-ray structures of MtFBA bound with DHAP, DHAP-G3P or FBP[2], or the apo MtFBA structure[9]. Specifically, the MtFBA-PGH complex maintains a typical β/α-barrel structure composed of an eight β-sheet core (β1-β8) surrounded by eight α-helices (α1-α8a; Figure 3a) [2]. Strikingly, well-ordered electron density within the active site was also observed for the previously elusive active site loop (residues 168-179; Figure 3b). This loop region is disordered in the X-ray structures of MtFBA bound with DHAP, DHAP-G3P, or FBP [2]. However, in the MtFBA-PGH complex, additional secondary structural elements are formed including a new β-strand (β5b), that forms an anti-parallel β-sheet with residues 166-169 (β5a), and a new 3_{10}-helix (3_{10}a) that completes the formation of the active site loop (Figure 3c,d).

In addition to the newly resolved active-site loop, electron density for a molecule of PGH, the active site metal cations (Zn^{2+} and Na^+), a zinc atom, an acetate molecule, and a molecule of PEG 300 are also observed in the asymmetric unit (Figure S2). The well-resolved acetate and PEG 300 molecules are both observed within a binding pocket that is distal to the active site of the enzyme. Within this pocket, there are several polar residues, including two lysine residues, that can facilitate the binding of these ligands. The location of this pocket and the presence of these lysines may be of significance in the interaction of human plasminogen with MtFBA that was recently suggested by de la Paz Santangelo et al. They reported that interactions between plasminogen and MtFBA are dependant on MtFBA lysines and independent of the MtFBA active site[9]. Since this pocket is the only sizable

cleft outside of the active site, and it contains the presence of lysines and binds ligands, this pocket might be a candidate for these MtFBA-plasminogen interactions.

MtFBA active site loop

The main chain density for the previously unresolved amino acids, 168-179, of MtFBA was readily observed from F_o-F_c electron density maps calculated after initial refinement Figure S1a). Upon building the missing backbone atoms of the loop residues into electron density, the majority of the side chain residues became immediately apparent (Figure 3b). Simulated annealing electron maps also revealed density for all residues of the loop except for expectedly flexible Gly171 located at the tip of the loop (Figure S1b,c). Formation of salt-bridges between E168/K309 and D170/R314 are observed suggesting that these interactions are important in anchoring β-strand β5 within the β-turn. These two interactions also result in lower B-factor values (<40 Å^2) for these residues, which helps produce complete side chain density for residues within β-strand β5a and the β-turn. In contrast, β-strand β5b is only held in place through only one, main chain β-sheet interaction, which results in significantly higher B-factors (40-90 Å^2) and less defined density for associated side chains (Figure 3b). The bound position of the active site loop forms a flap over the PGH-bound active site, which is distal to any dimer-dimer or intra-tetrameric interfaces. This orientation suggests that only intra-monomer and intra-dimer interactions are responsible for the stabilization of the loop in its closed form (Figures 3b,S2).

PGH-bound active site of MtFBA

A closer examination within the active site of the MtFBA-PGH bound structure reveals well-ordered electron density for PGH (Figure 4a). The hydroxyl group of PGH produces an oxygen-ZN1 bond length shorter than 2.2 Å, which is indicative of a first-coordination sphere bond with ZN1 (Figure 4b,c,d). The ketone oxygen (O-C in Figure 4b) of PGH forms a longer bond with ZN1 suggesting a near first-sphere H-bond interaction. As a result, ZN1 has a distorted trigonal bipyramidal coordination geometry that is similar to the coordination geometry surrounding the active site zinc atom in the MtFBA-DHAP structure (Figure 4b)[2, 30].

Although the interactions between MtFBA and PGH appear at first to be similar to those with the reaction intermediate, HEI, the newly observed and ordered conformation of the active site loop reveals additional interactions between MtFBA and PGH. These interactions are mediated through a newly observed active site water molecule, W57. This water molecule forms a 2.9 Å hydrogen bond with the hydroxamate nitrogen atom of PGH, and is coordinated to D276 and E169 through hydrogen bonds. D276 has been previously implicated in the stereo-selectivity of MtFBA for fructose-1,6-biphosphate enantiomers, and E169 is located within the active site loop (Figure 4c). The orientation of the E169 side chain and its coordination to a water molecule in a position to contribute to catalysis suggests that E169 is a catalytically relevant residue likely acting through a proton-shuttle mechanism.

X-ray Structure of substrate and product-free MtFBA

To probe how the binding of substrates and products influence the conformation of the active site loop and its interaction with the active site, and to rule out the possibility that DHAP could have co-purified with MtFBA and contributed to the observed loop density in the active site, MtFBA was crystallized in the absence of PGH or any other added MtFBA substrate/products. Crystals of the substrate-free and product-free form of the enzyme (MtFBA-holo), were grown using the same crystallization conditions as those that produced MtFBA-PGH crystals except that 2% DMSO was used as an additive. X-ray data were collected and the final data processing and statistics are summarized in Table 1. Inspection of the MtFBA active site in the absence of added substrates/products or inhibitor reveals that no ligands are bound except for an acetate molecule from the mother-liquor that coordinates to the active site sodium cation (Figure 5a). Additionally, well-ordered electron density for two water molecules that occupy the first-coordination sphere of the active site zinc cation (ZN1), are also observed (Figure 5). The coordination geometry surrounding the zinc atom in the active site of the MtFBA-holo enzyme is analogous to that of the EcFBA structure that was also determined in the absence of substrates and products (Figure 5a-c)[19]. The presence of the zinc in the active site also correlates with the observation of zinc in the active site of MtFBA reported by Labbé et al. (2011) who used biochemical approaches[31].

Interestingly, the active site zinc cation coordinating to the imidazole nitrogen of H212 was not observed in the active site of a MtFBA structure (MtFBA-NZ; pdb 4A21) that was recently determined to 2.3 Å[9]. This lower resolution structure was determined from crystals that were grown from significantly different crystallization conditions than those used here to determine the zinc and sodium cation bound form of MtFBA (Figure 5d)[9]. The crystallization and purification of MtFBA-NZ reported by de la Paz Santangelo et al. was achieved under high inhibitory concentrations of ammonium sulfate and lithium sulfate and in the absence of Zn^{2+}, which directly impacted the structure within the MtFBA active site[9]. Specifically, these conditions resulted in the binding of sulfate polyanions and an additional cation, presumably a sodium ion, which are bound in non-catalytically relevant positions. The identity of the additional cation as sodium, lithium, or ammonium was not independently confirmed[9]. As a result, the X-ray structure of the substrate and product free from of MtFBA reported here may better represent the holoenzyme, or near apoenzyme, form of MtFBA.

Probing the catalytic roles of residues within the MtFBA active site loop

The well-ordered structure of the active site loop in the MtFBA-PGH complex and the available kinetic information on the EcFBA loop-mutant enzymes reported by Berry and colleagues allowed us to propose possible catalytic roles for some of the same amino acids within this loop[22]. Therefore, we used site-directed mutagenesis to test whether E169 and E168 participate in the deprotonation/protonation reaction, and whether the flexibility of the two glycine residues (G166 and G167) at the beginning of the loop, influence the catalytic efficiency of MtFBA. In addition, we also characterized further the role of D276 in solvent-exchange in the deprotonation/protonation reaction[2, 17, 32, 33].

The steady-state kinetic parameters and deuterium solvent isotope effects on five MtFBA mutants were determined and the results are summarized in Table 2. The rate of FBP catalysis by MtFBA was measured using an NADH-coupled assay at room temperature and the maximal turnover number,k_{cat}, was determined to be 720 ± 10 min^{-1} for the wild type enzyme. This k_{cat} value is ~60% of the value reported for MtFBA by Ramsaywak et al. determined at 28°C, and ~50% of the value reported for MtFBA by Labbé et al. determined at 30°C[4, 31]. The corresponding increases of k_{cat} for MtFBA in response to increasing temperatures has also been reported by Rukseree et. al. providing a basis for the differences of k_{cat} between this study and others[4, 24, 31]. Beyond comparisons of k_{cat} determined for MtFBA from different studies, the k_{cat} value for MtFBA determined here is comparable to the value determined for EcFBA at 30°C (22). It is also approximately three times the k_{cat} value reported for GlFBA taken at a similar temperature [17, 21]. The K_m value for the interaction of FBP with MtFBA was determined to be 40 ± 1 μM and is consistent with the value for MtFBA determined previously[4]. However, the K_m value for MtFBA is an order of magnitude lower than that for the EcFBA enzyme and an order of magnitude greater than the K_m value for the GlFBA enzyme [17, 21, 22].

Many class II FBAs, including MtFBA, contain two glutamate residues in tandem within the active site loop, MtFBA E168 and E169 (Figure 3c). In the case of GlFBA and TaFBA, these two glutamates are off set from those of EcFBA, which has previously been proposed to be the residue responsible for protonation/deprotonation of DHAP in the FBP-cleavage reaction catalyzed by EcFBA[22]. Mutation of E169 to an alanine in MtFBA resulted in significant decreases in both k_{cat} (~1800-fold) and k_{cat}/K_m (~1000-fold) for the FBP-cleavage reaction, whereas mutation of nearby E168 to alanine only resulted in an approximate 5-fold decrease in k_{cat} from that of wild type MtFBA. These decreases support the MtFBA-PGH structure's assertion that E169 of MtFBA directly participates in the acid/base catalytic machinery associated with the active site loop. Also, these reductions in activity are significantly more profound than those observed for the EcFBA enzyme, k_{cat} (~315-fold) and k_{cat}/K_m (~600-fold), suggesting that E169 may be slightly more rate-limiting in the MtFBA catalyzed cleavage of FBP.

Additionally, a direct interaction between the carboxylate side-chain of E169 and a water molecule (#57 Figure 4c) that is directly hydrogen bonded to the hydroxamate nitrogen of PGH is clearly observed suggesting E169 serves as a proton shuttle that abstracts the C1 proton from DHAP (Figure 1a). In addition to the coordination of the active site water by the carboxylic side chain of E169, the carboxylic group of D276 also directly coordinates this water molecule. As observed in the MtFBA-FBP structure, D276 is expected to contribute to the binding of and stereo-selectivity for FBP. Therefore, it is not surprising that the alanine mutant, D276A, elevated the K_m 5-fold[2, 17]. Intriguingly, the D276A mutation also resulted in a 26-fold reduction in k_{cat}. This reduction in activity, along with the MtFBA-PGH evidence that D276 coordinates with an active site water molecule, suggests that D276's role goes beyond facilitating the binding of FBP.

We also probed the sensitivity of the FBP-cleavage reaction to solvent-derived deuterons by performing deuterium solvent-isotope effects. For the wild type MtFBA enzyme, a normal solvent isotope effect on ^DV, $(k_{cat}^H/k_{cat}^D = 1.9)$, is observed, whereas no solvent isotope

effect is observed on $^D(V/K)$, $(k_{cat}/K_m)^H/(k_{cat}/K_m)^D =0.94$, suggesting proton transfer is partially rate limiting in the ES complex (Table 2c). In contrast, normal solvent isotope effects are observed on both ^DV, $(k_{cat}^H/k_{cat}^D = 2.1)$, and $^D(V/K)$, $(k_{cat}/K_m)^H/(k_{cat}/K_m)^D)=2.5$, for E169A MtFBA. Also, significant solvent isotope effects are observed for single and double MtFBA loop mutants, $^D(V/K)$s, $(k_{cat}/K_m)^H/(k_{cat}/K_m))^D)=3.2$ and 3.5 respectively.

DISCUSSION

Roles of key active site loop residues of MtFBA

Previously, the inability to visualize the MtFBA active site loop left ambiguity as to which residues within this loop participate in the catalytic mechanism of MtFBA. Mutagenesis studies and primary kinetic isotope effects on the deprotonation of [1(S)-^{2}H] DHAP by Berry and coworkers conducted on EcFBA implicated residue E182 within the active site loop of EcFBA as being directly involved in the protonation/deprotonation step of the FBA mediated reaction[22]. However, direct structural proof of the interaction of E182 with substrates, intermediates or products could not be achieved as the active site loop was always disordered in X-ray structures. As in EcFBA, TaFBA, and GlFBA, MtFBA has two tandem glutamates, E168 and E169, within the active site loop. Furthermore, whether the glutamate directly acted on substrates of MtFBA or exerted its function through a water molecule was previously unclear. The MtFBA-PGH structure reported here provides insight into both these issues. Visualization of E169 within the MtFBA active site is experimentally clear, and the side chain of E169 coordinates a water molecule that is H-bonded to PGH. This observation clearly advocates E169 as the glutamate involved in protonation/ deprotonation in MtFBA and that it functions through a proton shuttle mechanism with a water molecule. Since this glutamate aligns with EcFBA E182 upon sequence comparison, and since its mutation to alanine resulted in the most catalytically hindered mutation between the two glutamates (Table 2a), these results corroborate the assignment by Berry and colleagues that E182 in EcFBA functions as the catalytic acid/base. Finally, the solvent isotope effects observed for the selected MtFBA mutants supports the importance of E169 in the catalytic mechanism.

For an enzyme to exhibit a solvent isotope effect, the rate-limiting step must involve the breaking or formation of bonds that involve solvent derived deuterons. For class II FBAs, this translates to the protonation/deprotonation steps[22]. Out of the wt and five mutant FBAs evaluated, only the E169A and MtFBA loop mutations that likely restrict E169 to be positioned in a catalytically relevant position, or that prevent E169 from being in the active site at all, exhibited a significant isotope effect $(((k_{cat}/K_m)^H/(k_{cat}/K_m)^D > 1$; Table 2). With no isotope effect observed for E168A, and a significant effect on k_{cat} for the E169A mutation, not only is the identity of E169 as the residue responsible for protonation/ deprotonation in MtFBA revealed, but also that protonation facilitated by E169 during FBP cleavage becomes more rate limiting in the E169A mutant. Unfortunately, these results could not be compared in total with those performed on EcFBA, as that study did not include an equivalent E168A mutant. However, these results do complement those obtained from EcFBA.

For EcFBA, primary isotope effects were measured for the reverse reaction with [1(S)-^{2}H] DHAP as the substrate, whereas we determined the solvent isotope effect of FBP cleavage by MtFBA. The mechanism of MtFBA suggests that up to five enzyme states may occur (Figure 1a). These five enzymes states comprise one for the holoenzyme as well as four others representing the different states of the ES and EP complexes (Figure 1b). Intriguingly, at least three steps, *2, 4*, and *5* (Figure 1b), are potentially sensitive to solvent isotope effects. Naturally, when glutamate is mutated to alanine, the mechanistic steps that utilize this residue will become more rate limiting (Table 2c). Interestingly, as in the EcFBA primary isotope study, no solvent isotope effect on ^{D}(V/K$_m$) for wild type MtFBA was observed suggesting that either the active site loop protonation/deprotonation is not the rate limiting step, or that the isotope effect on this step is masked by increases in the energy barriers of other solvent isotope sensitive steps (Figure 1b). A value of 1.93 for ^{D}V on wt MtFBA supports the latter explanation and suggests that the proton-transferring step facilitated by the side chain of E169 is partially rate-limiting.

Mechanism of MtFBA inhibition by PGH

Since DHAP was found to be a competitive inhibitor against FBP for MtFBA, the K$_i$ value derived from the kinetics studies is therefore a dissociation constant for DHAP from the MtFBA-DHAP complex. Comparison of the K$_d$ values for the DHAP-MtFBA and PGH-MtFBA complexes reveals a 11,333-fold increase in affinity of PGH over DHAP for MtFBA. The MtFBA-PGH structure and accompanying results of ITC and kinetic experiments support a possible mechanism for the increase in affinity. Unlike the extra density observed in the MtFBA-DHAP structure, which was accounted for by the presence of DHAP in addition to that of HEI intermediate, no such density is observed in the MtFBA-PGH active site (Figure 4a). This reinforces the assignment of PGH in the active site of MtFBA-PGH and the assertion that HEI is observed in the MtFBA-DHAP active site[2]. In contrast to the carbon 1 of HEI that forms an sp^2 hybridized orbital system in its coordination with ZN1, a geometry suggested by its 118° bond angle and the oxygen-zinc distances resembling two coordinating bonds, PGH adopts a tetrahedral sp^3 geometry with an angle of ~ 109° between PGH's nitrogen, its bound oxygen and the hydrogen bonded active site water (Figure 4c). Additionally, only the nitrogen-bound oxygen of PGH forms a coordinating bond with the catalytic zinc, whereas its carbon bound oxygen's bond with the catalytic zinc resembles a longer H-bond. This suggests that the PGH's carbon-bound oxygen is in a ketone form. This narrows the possible resonance species of PGH found within the MtFBA active site to two forms, **2** or **6**, in Figure 6a. Although the distance between the PGH hydroxyl oxygen atom and ZN1 favors the assignment of species **2** to PGH within the active site, the low pH of the crystallization solution would likely favor the protonated form of **2**, which is species **6** (Figure 5b)[34]. In either case, the interatomic distances between PGH, W57, E169 and D276, as well as tetrahedral geometry of the secondary amine, which includes the lone electron pair, suggests the formation of an H-bond network as depicted in Figure 6b. In this scheme, a lone pair of electrons on the secondary amine points toward the back of the MtFBA active site, while W57 forms H-bonds with D276 and E169. This facilitates W57's involvement of extracting a proton from PGH. However, as reflected in the types of bonds formed between ZN1 and PGH as well as PGH's electron configuration, the secondary amine is not polarized to allow proton extraction as

occurs with the hydroxymethylene hydrogen atoms of DHAP[2, 5]. Thus, the water molecule fails to strip the proton from PGH and instead forms a stable H-bond network between PGH, W57, D276 and E169. This network stabilizes the active site loop in a closed conformation preventing PGH from being readily exchanged with MtFBA substrates likely contributing to PGH's robust inhibitory properties.

The isoelectronic similarity between DHAP and PGH suggests that they should block the same space in the MtFBA active site from FBP binding or displace the same two waters observed in the MtFBA-holo active site (Figure 5a). As a result, they both would have the same entropic component for binding. However, PGH possesses a vastly higher affinity for MtFBA than DHAP. This implies a significant disparity in enthalpic contributions of binding between the DHAP and PGH, which is in line with the significant heat associated with PGH binding to MtFBA and the lack of heat associated with DHAP binding observed in ITC experiments (Figure 2). The heat observed from the binding of PGH suggests formation of stable bonds between MtFBA and PGH, which are not present between MtFBA and DHAP. Comparison of the MtFBA-DHAP and MtFBA-PGH structures bear this out with three anti-parallel β-sheet H-bonds, two salt-bridges and a network of H-bonds between E169, a water molecule, D276 and PGH formed in the MtFBA-PGH structure, whereas no density for active site loop is found in the MtFBA-DHAP structure[2]. As both the MtFBA-DHAP and MtFBA-PGH complexes possess the capability of forming similar inter-MtFBA interactions, the interaction with E169 and PGH appears to be the discerning factor in stabilizing the active site loop in MtFBA.

Previous structural studies of class II FBAs utilized PGH to mimic HEI but were unable to observe the active site loop and any additional interactions that modulate loop stabilization beyond those formed directly by PGH and active site waters[5, 13, 17]. In the case of MtFBA, these interactions are formed by two salt-bridges between D170/D314 and E168/K308 (Figure 3b). As class IIb FBAs, both GlFBA and HpFBA lack the equivalent K309 of MtFBA as well as the presence of an isoleucine or aspartic acid residue inserted in the active site loop just prior to the active loop glutamates[13, 17]. As a class IIa FBA, EcFBA does have the conserved residues that could potentially form these salt-bridges to stabilize the loop in a catalytically relevant orientation. However, high concentrations of zinc, 2-5 mM, were used to determine the EcFBA-PGH structure, and this may have artificially created an additional zinc-binding site near EcFBA's active site loop. This additional zinc site was not observed in the MtFBA structures elucidated in the presence of 0.1 mM zinc. The additional zinc found in EcFBA, may have altered EcFBA-PGH's active site by forming a bond with E181 orienting E182 to form a salt-bridge with EcFBA's R334[5]. Consequently, EcFBA-PGH's active site loop may have been prevented from adopting an orientation similar to that of in the MtFBA-PGH's active site loop[2]. Another possibility for being able to trap the active site loop of MtFBA with PGH bound is the pH of the crystallization solution. Whereas MtFBA-PGH was crystallized under mildly acidic conditions, the structures of EcFBA-PGH, GlFBA-PGH, and HpFBA-PGH structures were all resolved in mildly basic conditions[5, 13, 17]. However, the MtFBA-DHAP-HEI structure was crystallized under the same conditions as those for crystallization of the MtFBA-PGH complex and, similar to EcFBA-PGH and GlFBA-PGH, no electron density was observed for the active site loop. Additionally, a mixture of the substrate, DHAP, and the reaction intermediate, HEI, was

found in the active site of MtFBA co-crystallized with an excess concentration of DHAP suggesting that under MtFBA-PGH crystallization conditions, proton transfer can still occur[2]. Overall, these observations suggest that the presence of PGH, and possibly the greater presence of protonated water within the MtFBA-PGH active site, may contribute to the stability of the active site loop in a closed state.

In conclusion, through X-ray crystallographic visualization of the potent inhibitor PGH bound to the active site of the MtFBA enzyme, significant insight into the contribution of the active site loop to the catalytic mechanism of protonation/deprotonation in class II FBAs can now be envisioned. Additionally, key active site loop residues in MtFBA, specifically E169 and a catalytic water molecule, have been identified. As a result, a greater understanding of how class II FBAs perform this critical step in the cleavage of FBP into DHAP and G3P has been achieved. The MtFBA-PGH structure also illustrates a mechanism that explains the three-orders of magnitude increase in affinity of PGH over DHAP for the active sites of FBAs. PGH's ability to form favorable active site loop stabilizing interactions to elicit this increase in affinity, underlines the importance and necessity of developing inhibitors that possess similar interactions with bacterial class II FBA active site loops.

Acknowledgments

References

1. Marsh JJ, Lebherz HG. Fructose-bisphosphate aldolases: an evolutionary history. Trends Biochem Sci. 1992; 17:110–113. [PubMed: 1412694]

2. Pegan SD, Rukseree K, Franzblau SG, Mesecar AD. Structural basis for catalysis of a tetrameric class IIa fructose 1,6-bisphosphate aldolase from Mycobacterium tuberculosis. J Mol Biol. 2009; 386:1038–1053. [PubMed: 19167403]

3. Rutter WJ. Evolution of Aldolase. Fed Proc. 1964; 23:1248–1257. [PubMed: 14236133]

4. Ramsaywak PC, Labbe G, Siemann S, Dmitrienko GI, Guillemette JG. Molecular cloning, expression, purification, and characterization of fructose 1,6-bisphosphate aldolase from Mycobacterium tuberculosis--a novel Class II A tetramer. Protein Expr Purif. 2004; 37:220–228. [PubMed: 15294302]

5. Hall DR, Leonard GA, Reed CD, Watt CI, Berry A, Hunter WN. The crystal structure of Escherichia coli class II fructose-1, 6-bisphosphate aldolase in complex with phosphoglycolohydroxamate reveals details of mechanism and specificity. J Mol Biol. 1999; 287:383–394. [PubMed: 10080900]

6. Gerdes SY, Scholle MD, Campbell JW, Balazsi G, Ravasz E, Daugherty MD, Somera AL, Kyrpides NC, Anderson I, Gelfand MS, Bhattacharya A, Kapatral V, D'Souza M, Baev MV, Grechkin Y, Mseeh F, Fonstein MY, Overbeek R, Barabasi AL, Oltvai ZN, Osterman AL. Experimental

determination and system level analysis of essential genes in Escherichia coli MG1655. J Bacteriol. 2003; 185:5673–5684. [PubMed: 13129938]

7. Baba T, Ara T, Hasegawa M, Takai Y, Okumura Y, Baba M, Datsenko KA, Tomita M, Wanner BL, Mori H. Construction of Escherichia coli K-12 in-frame, single-gene knockout mutants: the Keio collection. Mol Syst Biol. 2006; 2:2006 0008.

8. Wehmeier UF. Molecular cloning, nucleotide sequence and structural analysis of the Streptomyces galbus DSM40480 fda gene: the S. galbus fructose-1,6-bisphosphate aldolase is a member of the class II aldolases. FEMS Microbiol Lett. 2001; 197:53–58. [PubMed: 11287146]

9. de la Paz Santangelo M, Gest PM, Guerin ME, Coincon M, Pham H, Ryan G, Puckett SE, Spencer JS, Gonzalez-Juarrero M, Daher R, Lenaerts AJ, Schnappinger D, Therisod M, Ehrt S, Sygusch J, Jackson M. Glycolytic and non-glycolytic functions of Mycobacterium tuberculosis fructose-1,6-bisphosphate aldolase, an essential enzyme produced by replicating and non-replicating bacilli. J Biol Chem. 2011; 286:40219–40231. [PubMed: 21949126]

10. Bai NJ, Pai MR, Murthy PS, Venkitasubramanian TA. Effect of oxygen tension on the aldolases of Mycobacterium tuberculosis H37Rv. FEBS Lett. 1974; 45:68–70. [PubMed: 4213059]

11. Scamuffa MD, Caprioli RM. Comparison of the mechanisms of two distinct aldolases from Escherichia coli grown on gluconeogenic substrates. Biochim Biophys Acta. 1980; 614:583–590. [PubMed: 6996735]

12. Rosenkrands I, Slayden RA, Crawford J, Aagaard C, Barry CE 3rd, Andersen P. Hypoxic response of Mycobacterium tuberculosis studied by metabolic labeling and proteome analysis of cellular and extracellular proteins. J Bacteriol. 2002; 184:3485–3491. [PubMed: 12057942]

13. Fonvielle M, Coincon M, Daher R, Desbenoit N, Kosieradzka K, Barilone N, Gicquel B, Sygusch J, Jackson M, Therisod M. Synthesis and biochemical evaluation of selective inhibitors of class II fructose bisphosphate aldolases: towards new synthetic antibiotics. Chemistry. 2008; 14:8521–8529. [PubMed: 18688832]

14. Global tuberculossis control -surveillance, planning, financing. World Health Organization; Geneva, Switzerland: 2008. p. 1-5.

15. Tuberculosis MDR-TB & XDR-TB. World Health Organization; Geneva, Switzerland: 2008.

16. Collins KD. An activated intermediate analogue. The use of phosphoglycolohydroxamate as a stable analogue of a transiently occurring dihydroxyacetone phosphate-derived enolate in enzymatic catalysis. J Biol Chem. 1974; 249:136–142. [PubMed: 4588689]

17. Galkin A, Li Z, Li L, Kulakova L, Pal LR, Dunaway-Mariano D, Herzberg O. Structural insights into the substrate binding and stereoselectivity of giardia fructose-1,6-bisphosphate aldolase. Biochemistry. 2009; 48:3186–3196. [PubMed: 19236002]

18. Fonvielle M, Weber P, Dabkowska K, Therisod M. New highly selective inhibitors of class II fructose-1,6-bisphosphate aldolases. Bioorg Med Chem Lett. 2004; 14:2923–2926. [PubMed: 15125960]

19. Cooper SJ, Leonard GA, McSweeney SM, Thompson AW, Naismith JH, Qamar S, Plater A, Berry A, Hunter WN. The crystal structure of a class II fructose-1,6-bisphosphate aldolase shows a novel binuclear metal-binding active site embedded in a familiar fold. Structure. 1996; 4:1303–1315. [PubMed: 8939754]

20. Izard T, Sygusch J. Induced fit movements and metal cofactor selectivity of class II aldolases: structure of Thermus aquaticus fructose-1,6-bisphosphate aldolase. J Biol Chem. 2004; 279:11825–11833. [PubMed: 14699122]

21. Galkin A, Kulakova L, Melamud E, Li L, Wu C, Mariano P, Dunaway-Mariano D, Nash TE, Herzberg O. Characterization, kinetics, and crystal structures of fructose-1,6-bisphosphate aldolase from the human parasite, Giardia lamblia. J Biol Chem. 2007; 282:4859–4867. [PubMed: 17166851]

22. Zgiby S, Plater AR, Bates MA, Thomson GJ, Berry A. A functional role for a flexible loop containing Glu182 in the class II fructose-1,6-bisphosphate aldolase from Escherichia coli. J Mol Biol. 2002; 315:131–140. [PubMed: 11779234]

23. Weber P, Fonvielle M, Therisod M. New facile synthesis of phosphoglycolohydroxamic acid and other phosphoglycolic acid derivatives. Tetrahedron Letters. 2003; 44:9047–9049.

24. Rukseree K, Thammarongtham C, Palittapongarnpim P. One-step purification and characterization of a fully active histidine-tagged Class II fructose-1,6-bisphosphate aldolase from Mycobacterium tuberculosis. Enzyme and Microbial Technology. 2008; 43:500–506.

25. Gill S, Hippel Pv. Calculation of protein extinction coefficients from amino acid sequence data. Analytical Biochemistry. 1989; 182:319–326. [PubMed: 2610349]

26. Krezel A, Bal W. A formula for correlating pKa values determined in D2O and H2O. J Inorg Biochem. 2004; 98:161–166. [PubMed: 14659645]

27. Otwinowski, Z.; Minor, W. Macromolecular Crystallography, Part A. Vol. 276. Academic Press; New York: 1997. Processing of X-ray Diffraction Data Collected in Oscillation Mode.

28. The CCP4 suite: programs for protein crystallography. Acta crystallographica Section D Biological crystallography. 1994; 50:760–763.

29. Adams PD, Afonine PV, Bunkoczi G, Chen VB, Davis IW, Echols N, Headd JJ, Hung LW, Kapral GJ, Grosse-Kunstleve RW, McCoy AJ, Moriarty NW, Oeffner R, Read RJ, Richardson DC, Richardson JS, Terwilliger TC, Zwart PH. PHENIX: a comprehensive Python-based system for macromolecular structure solution. Acta crystallographica Section D Biological crystallography. 2010; 66:213–221.

30. Alberts IL, Nadassy K, Wodak SJ. Analysis of zinc binding sites in protein crystal structures. Protein Sci. 1998; 7:1700–1716. [PubMed: 10082367]

31. Labbe G, de Groot S, Rasmusson T, Milojevic G, Dmitrienko GI, Guillemette JG. Evaluation of four microbial Class II fructose 1,6-bisphosphate aldolase enzymes for use as biocatalysts. Protein Expr Purif. 2011; 80:224–233. [PubMed: 21763425]

32. Zgiby SM, Thomson GJ, Qamar S, Berry A. Exploring substrate binding and discrimination in fructose1, 6-bisphosphate and tagatose 1,6-bisphosphate aldolases. Eur J Biochem. 2000; 267:1858–1868. [PubMed: 10712619]

33. Hall DR, Bond CS, Leonard GA, Watt CI, Berry A, Hunter WN. Structure of tagatose-1,6-bisphosphate aldolase. Insight into chiral discrimination, mechanism, and specificity of class II aldolases. J Biol Chem. 2002; 277:22018–22024. [PubMed: 11940603]

34. Roos AK, Burgos E, Ericsson DJ, Salmon L, Mowbray SL. Competitive inhibitors of Mycobacterium tuberculosis ribose-5-phosphate isomerase B reveal new information about the reaction mechanism. J Biol Chem. 2005; 280:6416–6422. [PubMed: 15590681]

35. Harris TK, Abeygunawardana C, Mildvan AS. NMR studies of the role of hydrogen bonding in the mechanism of triosephosphate isomerase. Biochemistry. 1997; 36:14661–14675. [PubMed: 9398185]

Abbreviations

BSA	bovine serum albumin
CHA	cyclohexylamine
DHAP	dihydroxyacetone phosphate
DMSO	dimethyl sulfoxide
EcFBA	*Escherichia coli* class II fructose 1,6-bisphosphate aldolase
FBP	fructose 1,6-bisphosphate
GlFBA	*Giardia lambia* class II fructose 1,6-bisphosphate aldolase
G3P	glyceraldehyde 3-phosphate
HEI	hydroxyenolate intermediate
HEPES	N-2-hydroxyethylpiperazine-N'-2-ethane sulfonate

|	
HpFBA	*Helicobacter pylori* class II fructose 1,6-bisphosphate aldolase
ITC	isothermal titration calorimetry
IPTG	isopropyl-β-D-thiogalactoside
LB	Luria-Bertani
MtFBA	*Mycobacterium tuberculosis* class II fructose 1,6-bisphosphate aldolase
PGA	phosphoglycolamide
PGH	phosphoglycolohydroxamate
NADH	nicotinamide adenine dinucleotide
NMR	nuclear magnetic resonance
PEG	polyethylene glycol
PCR	polymerase chain reaction
SDS-PAGE	sodium dodecyl sulfate-polyacrylamide gel electrophoresis
TaFBA	*Thermus aquaticus* class II fructose 1,6-bisphosphate aldolase
TIM	triose phosphate isomerase
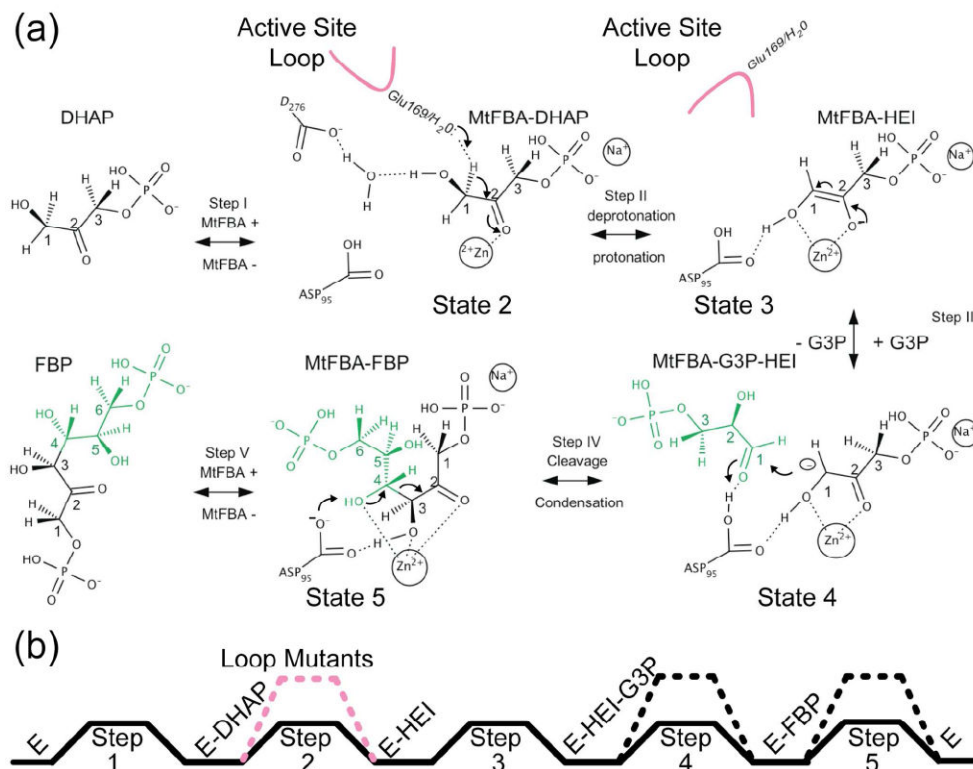
Figure 1. Proposed mechanism and reaction coordcinate of MtFBA
(a) A five-step, reversible chemical mechanism of MtFBA is shown along with associated structural motion of the active site loop. Atoms of FBP, that originated from G3P, are colored green for clarity and a pink line denotes the active site loop amino acids (168-179) of MtFBA. **(b)** Simplified reaction coordinate diagram for the MtFBA catalyzed reaction illustrating intermediate and transition states. The dashed lines represent reaction steps that involve proton transfer steps where possible increases in energy of the reaction barriers could occur due to these steps being sensitive to deuterium substitution.
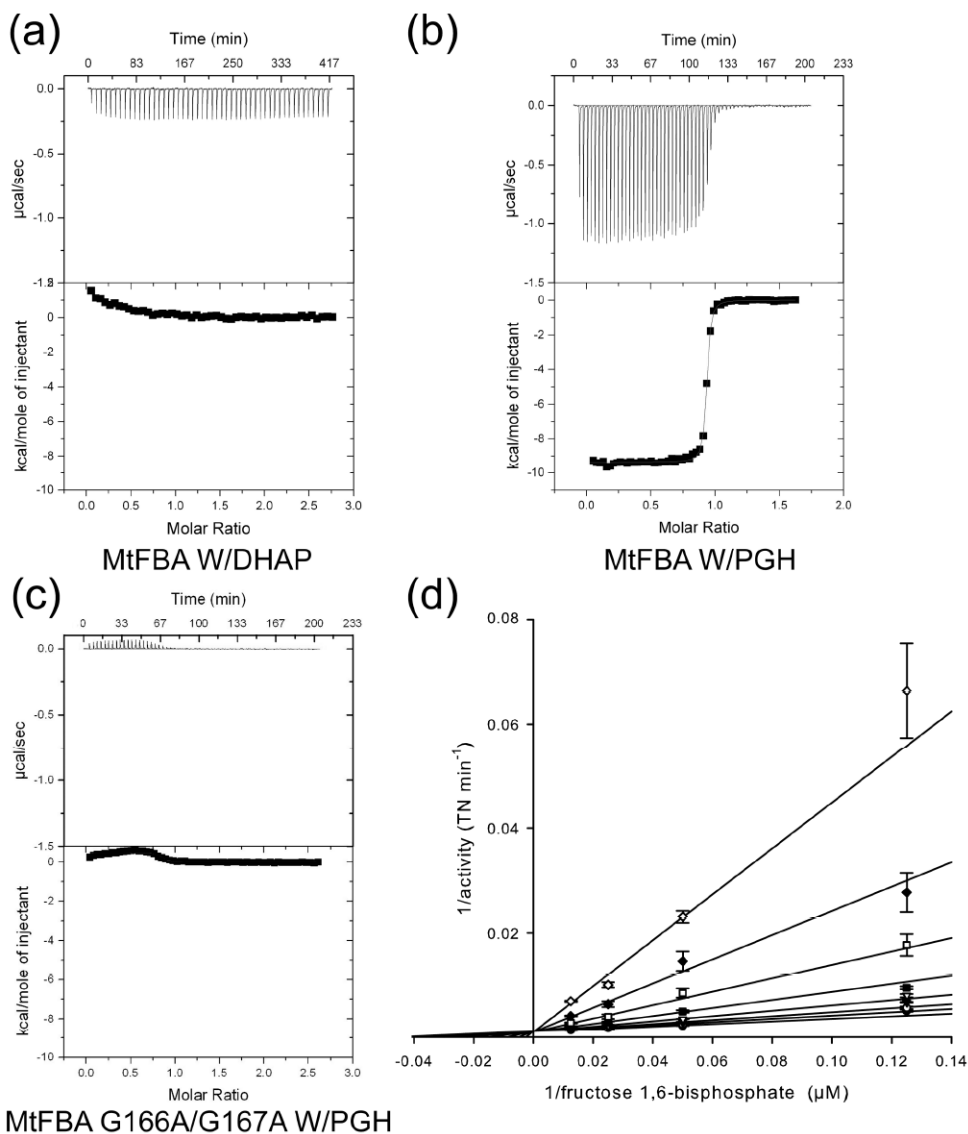
Figure 2. ITC and kinetic studies on the binding interactions of wild type and G166A/G167A MtFBA with PGH and DHAP

ITC thermographs (Upper Panels) and associated binding isotherms (Lower Panels) of wild type and mutant MtFBA titrated with either DHAP or PGH are shown in panels **a** thru **c**. (**a**) Wild type MtFBA titrated with DHAP. (**b**) Wild type MtFBA titrated with PGH. Data were fit to a single-site binding model using a monomeric concentration of MtFBA (lower panel). The resulting thermodynamic parameters and the value for n are given in the text. (**c**) G166A/G167A mutant MtFBA titrated with PGH. (**d**) Lineweaver-Burke Plot of DHAP inhibition of MtFBA. DHAP concentrations were: (●) 0 μM, (○) 62.5 μM, (▼) 125 μM, (▽) 250 μM, (.) 500 μM, (□) 1,000 μM, (◆) 2,000 μM, (◇) 4,000 μM. Data were globally fit to a pure competitive inhibition model. The resulting kinetic parameters are given in the text.
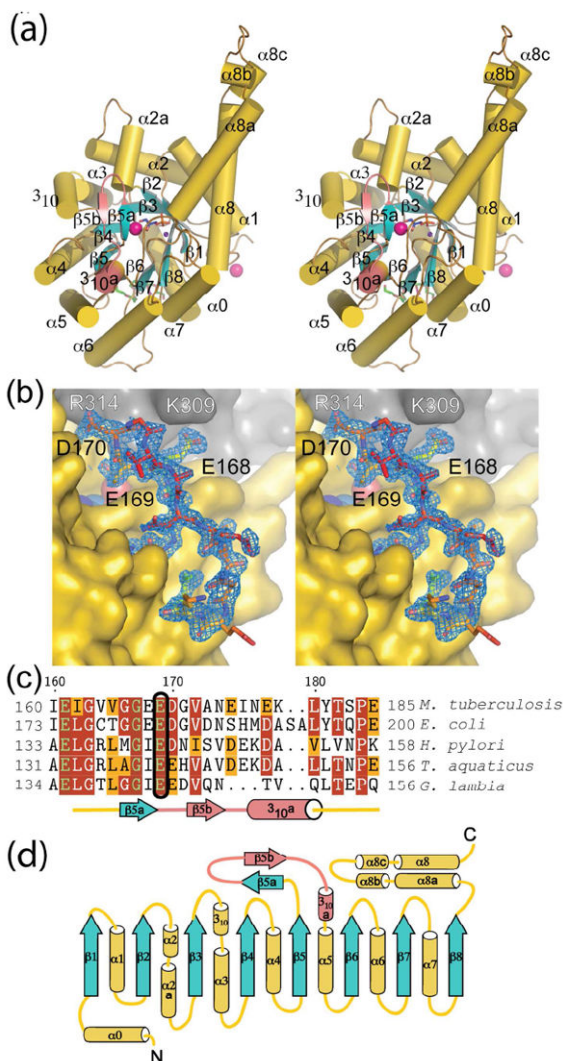
Figure 3. X-ray Structure of MtFBA aldolase in complex with PGH highlighting the newly resolved active site loop

(a) Divergent-eyed stereo view of a cartoon rendering of MtFBA-PGH protomer. Helical regions are presented as cylinders with β-strands as arrows. Helices and loops are colored in yellow with strands in light blue. Zinc ions (hot pink) are space fill rendered according to atomic radii with the active site sodium ion removed for clarity of PGH (blue) bound. Other ligands observed, PEG300 (green) and acetate (lavender), are present in stick form. Active site loop residues 168-179 are depicted in pink. **(b)** Divergent-eyed stereo view of MtFBA active site loop. MtFBA residues 165-180 are rendered in stick. Residues in stick are colored according to B-factors with blue representing a B-factor of ~25 to red representing a B-factor of ~90. PGH is depicted in CPK with carbons colored in cyan. All other residues are represented as a surface rendering with the asymmetric protomer in yellow and symmetry related surface in grey. Blue mesh reflects $2F_o$-F_c density maps calculated for the active site loop and contoured to 1 σ. **(c)** Sequence alignment of active site loop region of class IIa-b FBP aldolase from the H37RV strain of *M. tuberculosis* (protein accession NP_334786), *E. coli* (PDB 1B57_A), *H. pylori* (PDB 3C4U), *T. aquaticus* (PDB 1RV8_A), *G. lambia* (PDB

2ISV_A). Alignment generated using CLUSTALW, TEXSHADE, and BL2SEQ programs (http://workbench.sdsc.edu/) were used with the Matrix = BLOSUM62, Gap Opening Penalty = 11, Gap Extension Penalty = 1, and Lambda Ratio = 0.85. Amino acids are color coded according to being non-conserved (white), similar (orange), conserved (red), and completely conserved (red; green lettering) across the six sequences. Active site catalytically relevant glutamates circled. **(d)** Complete secondary structure topology of MtFBA. Secondary elements are colored as in (a).
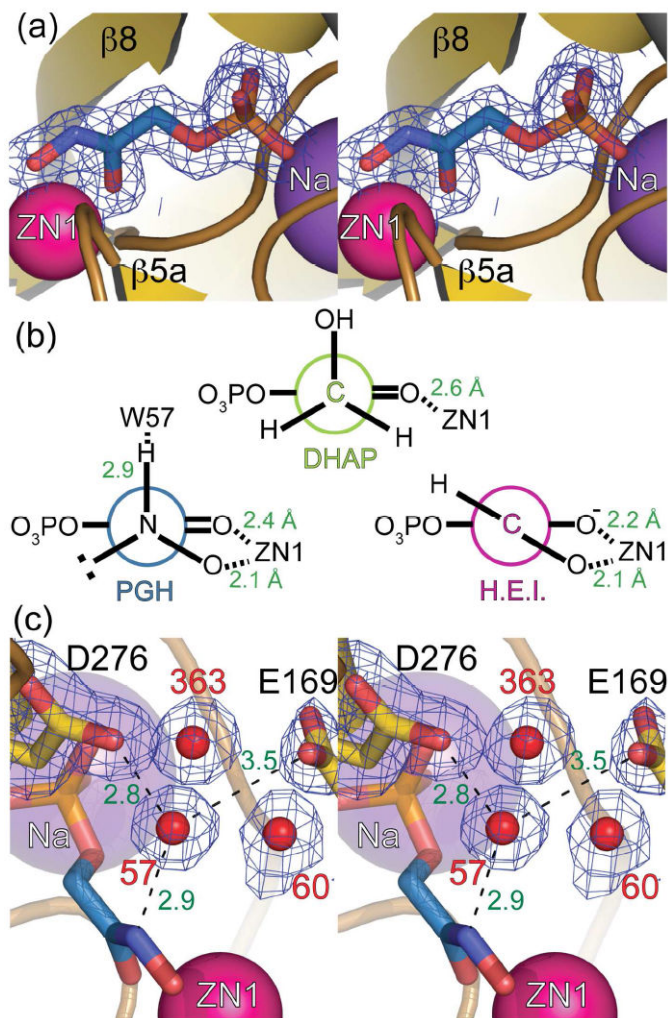
Figure 4. Structure of the MtFBA active site bound with PGH

(a) Divergent-eyed stereo view of the MtFBA active site bound with PGH (blue). The carbon atoms of the single protomer within the asymmetric unit are colored yellow. Heteroatoms are colored according to their element. Zinc (hot pink) and sodium (purple) ions are rendered in spheres according to their atomic size. The blue mesh represents the $2F_o$-F_c electron density maps surrounding the PGH molecule. The map is contoured to 1 σ. **(b)** Newman projection of DHAP, HEI, and PGH bound to a zinc cation (SN1) within the MtFBA active site. DHAP and HEI are from PDB entry 3KEL, and PGH is from PDB entry 4DEL. Intermolecular distances between the atoms of the bound ligands and ZN1 are shown in green. These illustrate the tetrahedral molecular geometry of PGH's nitrogen, which is divergent from HEI's trigonal planar geometry. **(c)** Divergent-eyed stereo alternate angle view of MtFBA active site with PGH bound. Labels of MtFBA-PGH residues are in black with labels for waters in red. All other atoms are rendered as in (a) and (b). H-bonds distances between W57, PGH, and MtFBA active site residues is colored in green.
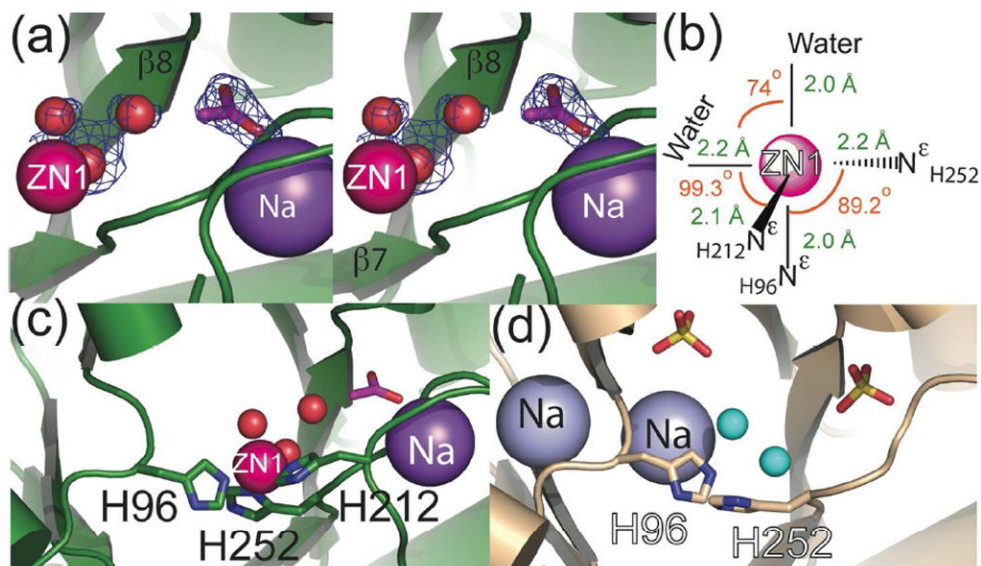
Figure 5. Active site structure of the MtFBA-holo enzyme
(a) Divergent-eyed stereo view of MtFBA-apo active site. Asymmetric unit protomer carbons are green heteroatoms are colored according to their element. Zinc (hot pink) and sodium (purple) ions are rendered in sphere according to atomic size. Waters (red) are depicted as spheres scaled to 50% for clarity. Electron density, $2F_o$-F_c map (blue) calculated at 1 σ around waters and acetate (lavender) located within the active site. **(b)** Coordination schematic of ZN1 in MtFBA-apo. Distances are in green with angles in orange. **(c)** MtFBA-apo active site. All atoms illustrated as in (a). Acetate ion (magenta) is rendered in stick form. **(d)** MtFBA with no active site zinc bound (4A21). Sodium (lavender) ions are rendered in sphere according to atomic size. Waters (cyan) are depicted as spheres scaled to 50% for clarity with sulfate anions rendered in stick form.
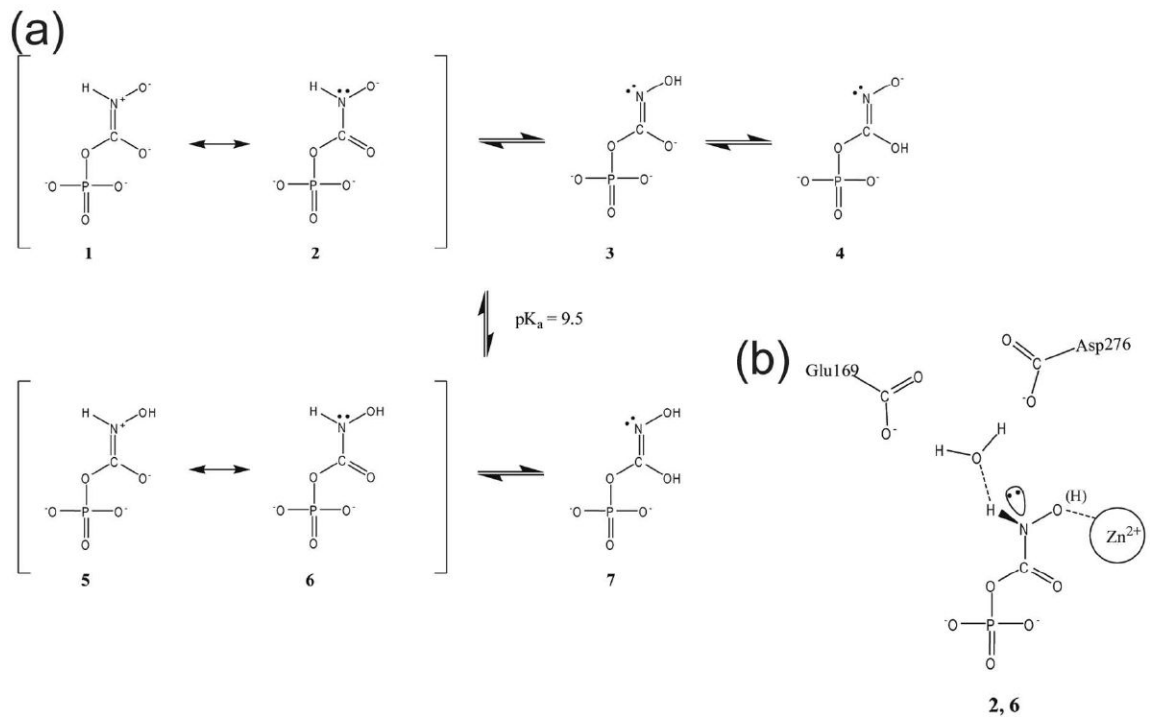
Figure 6. Ionization and Tautomeric forms of PGH in solution or in the MtFBA active site
(**a**) Plausible forms of PGH in solution under various pH conditions[35]. (**b**) Coordination of PGH within the MtFBA active site.

Table 1

Data Collection and Refinement

	MtFBA-PGH	MtFBA-APO
Data Collection		
Space Group	I222	I222
Unit Cell Dimensions		
a, b, c (Å)	61.8, 119.6, 164.0	60.7, 119.7, 164.8
$\alpha=\beta=\gamma(°)$	90	90
Resolution (Å)	93.90-1.58	96.9-1.64
No. Reflections Observed	354,909	158,675
No. Unique Reflections	78,320	65,340
R_{merge} (%)[a]	5.9 (27.9)[*]	4.5 (20.0)[*]
I/σI	22.6 (4.2)[*]	15.7 (4.4)[*]
% Completeness	94.0 (77.5)[*]	88.6 (94.8)[*]
Refinement		
Resolution Range	93.90-1.58	96.9-1.64
No. Reflections in Working Set	74,297	62,029
No. Reflections in Test Set	3,910	3,306
R_{work} (%)[b]	18.8	18.9
R_{free} (%)[b]	20.5	19.9
RMS deviation:		
Bond Lengths (Å)	0.01	0.01
Bond Angles (°)	1.2	1.1
Protein / Water Atoms	2738 / 580	2444 / 424
Average B-Factors ($Å^2$)		
Total	24.0	29.4
Protein	18.4	27.0
Water	40.4	43.6
Ligands	24.0	46.3
Ions	20.0	39.7

[*] The last resolution shell is shown in parentheses.

[a] $R_{merge}=\Sigma_h\Sigma_I |I_I(h) - <I(h)>| / \Sigma_h\Sigma_i I_I(h)$, where $I_I(h)$ is the ith measurement and $<I(h)>$ is the weighted mean of all measurements of $I(h)$.

[b] R_{work} and R_{free} = $h(|F(h)_{obs}| - |F(h)_{calc}|) / h|F(h)_{obs}|$ for reflections in the working and test sets, respectively. R.m.s., root mean square.

<div align="center">**Table 2**</div>

Kinetic Parameters for MtFBA

A: Fructose 1,6-bisphosphate (H_2O)[a]

Enzyme	$^c k_{cat}$ (min^{-1})	K_m (μM)	$^d k_{cat}/Km$ (μM^{-1} min^{-1})
wt	720 ± 10	40 ± 1	18 ± 1
E169A	0.40 ± 0.04	18 ± 1	0.017 ± 0.002
E168A	160 ± 10	30 ± 2	5.3 ± 0.5
G167A	10 ± 1	21 ± 1	0.48 ± 0.05
G167A, G166A	6.6 ± 0.1	21 ± 2	0.32 ± 0.03
D276A	27 ± 1	180 ± 10	0.15 ± 0.01

B: Fructose 1,6-bisphosphate (D_2O)[b]

Enzyme	k_{cat} (min^{-1})	K_m (μM)	k_{cat}/K_m (μM^{-1} min^{-1})
wt	370 ± 10	19 ± 1	19 ± 1
E169A	0.16 ± 0.01	14 ± 1	0.011 ± 0.001
E168A	50 ± 0.5	5.9 ± 0.5	8.7 ± 0.7
G167A	3.0 ± 0.1	20 ± 1	0.15 ± 0.01
G167A, G166A	1.9 ± 0.1	13 ± 1	0.15 ± .01
D276A	34 ± 1	180 ± 10	0.19 ± 0.01

C: Isotope Effect Relationships

Enzyme	k_{cat}^H/k_{cat}^D	K_m^H/K_m^D	$(k_{cat}/K_m)^H/(k_{cat}/K_m)^D$
wt	1.9 ± 0.1	2.1 ± 0.2	0.94 ± 0.07
E169A	2.5 ± 0.3	1.3 ± 0.2	2.0 ± 0.3
E168A	3.2 ± 0.2	5.1 ± 0.5	0.61 ± 0.07
G167A	3.2 ± 0.4	1.1 ± 0.1	3.20 ± 0.4
G167A, G166A	3.5 ± 0.2	1.6 ± 0.16	2.13 ± 0.24
D276A	0.80 ± 0.03	1.02 ± 0.06	0.79 ± 0.06

[a] The steady-state kinetic parameters were determined in 100 mM Tris-HCl, 100 mM potassium acetate, 0.4 mM NADH (pH 7.4) at 24 °C.

[b] The steady-state kinetic parameters were determined in 100 mM-Tris HCl, 100 mM potassium acetate, 0.4 mM NADH (pH 7.8/pD 7.4) at 24 °C.

[c] Errors are for k_{cat} and K_m are from the fit.

[d] Errors from k_{cat}/K_m and those of $(k_{cat}/K_m)^H/(k_{cat}/K_m)^D$ were calculated using $D(A/B) = (A/B) \sqrt{(DA/A)^2 + (DB/B)^2}$ with DA and DB representing the errors of A and B respectively.